Toward the prediction of Temperature Fluctuations by means of Steady RANS for the Estimation of Thermal Fatigue

Annalisa Manera[a], Horst-Michael Prasser[a,b]
[a]Paul Scherrer Institut, 5232 Villigen PSI, Switzerland
[b]ETHZ, Sonneggstrasse 3, 8092 Zurich, Switzerland
annalisa.manera@psi.ch; hprasser@ethz.ch

Richard Lechner, Thomas Frank
ANSYS Germany GmbH
Staudenfeldweg 12, D-83624 Otterfing, Germany
Richard.Lechner@ansys.com; Thomas.Frank@ansys.com

ABSTRACT

The prediction of thermal fatigue caused by mixing of fluid streams with different temperature needs fluid-dynamics simulations for the correct estimation of the temperature fluctuations in the wall which is exposed to the temperature patterns generated within this fluid. Currently, most of the efforts in this field are focused on the application of large eddy simulations (LES), which have the disadvantage of high CPU-time requirements and are therefore limited to relatively small geometries.
In this paper an attempt to predict temperature fluctuations by means of steady-state RANS simulations is presented. At this aim, the Reynolds stress equations are solved together with a transport equation for the temperature fluctuations. The great advantage of this approach lies in the considerably lower computational requirements if compared to LES and unsteady RANS, therefore allowing the application to more complex and larger geometries, such as the upper and lower head of a reactor pressure vessel. The model is validated against a T-junction experiment performed at the Paul Scherrer Institute, where the mixing patterns between water streams is measured by means of advanced instrumentation with high temporal and spatial resolution, providing transport scalar fluctuations for the validation of the theoretical model. Future efforts will be dedicated to the prediction of the fluctuations frequency, that combined with the fluctuations intensities, provide the boundary conditions for the analyses of thermal stresses in the structures.

KEYWORDS

Thermal fatigue, mixing, RANS, RSM, CFD, T-junction

1. INTRODUCTION

The mixing of fluid streams with different temperature may cause thermal fatigue in the walls of pressurized power plant equipment. Analyses require a correct estimation of the temperature fluctuations in the wall that is exposed to the temperature patterns generated within the fluid. Currently, most of the efforts in this field are focused on large eddy simulations (LES) [1-6]. These calculations provide temperature histories in the fluid, which allows to determinate both the amplitude and the power spectrum of the fluctuations. Existing applications are focused on the mixing phenomenon in T-junctions where the huge

computational efforts connected with this approach are still bearable. For more complex geometries it is desirable to search for alternative methods based on more efficient steady-state RANS models. A promising approach consists in the application of the so-called temperature fluctuation transport model, which can be coupled to a Reynolds stress model. The model is based on a second averaging of the scalar transport equation, which results in additional transport equations for the RMS of the scalar, i.e. the temperature, and the turbulent diffusion terms, which are averaged products of the temperature fluctuations with the fluctuations of each of the components of the velocity vector. This type of methodology has the clear advantage of being considerably less computational intensive than LES. ANSYS CFX 11.0 offers the possibility to activate the temperature fluctuation model as a hidden beta feature [7]. In the present article the model performances are evaluated against experimental results obtained in the T junction experiment of the Paul Scherrer Institute. There, the temperature as transport scalar was substituted by the concentration of salts affecting the electrical conductivity of the fluid. Wire-mesh sensors installed at different locations downstream of the side branch connection allow the measurement of two-dimensional distributions of the conductivity, which are transformed into concentration data allowing to analyze fluctuations of the transport scalar in a wide frequency range and with a 3 mm spatial resolution. The highly detailed experimental data permit to carrying out a comprehensive comparison with the theoretical model.

2. THEORETICAL MODEL

The methodology consists in the application of a Reynolds stress model, in combination with the energy equation for the evaluation of the temperature distribution, and an additional equation for the temperature turbulent fluctuations [7]. For the comparison with the experiments, a dimensionless scalar is defined from both calculated temperatures and measured conductivities, based on the assumption that both physical quantities behaves similarly with regard to turbulent mixing.

The momentum equation and the energy equation for incompressible fluids are respectively:

$$\frac{\partial(\rho U_i)}{\partial t}+\frac{\partial(\rho U_j U_i)}{\partial x_j}=-\frac{\partial P}{\partial x_i}-\frac{\partial(-\rho\tau_{ij}+\rho\overline{u_i u_j})}{\partial x_j} \tag{1}$$

$$\frac{\partial}{\partial t}(\rho H)+\frac{\partial}{\partial x_j}(\rho U_j H)=-\frac{\partial}{\partial x_j}\left(Q_j+\rho\overline{u_j h}\right) \tag{2}$$

where the closure problem clearly arises from the Reynolds stresses $\overline{u_i u_j}$ in eq. (1) and the turbulent heat fluxes $\overline{u_j h}$ in eq. (2). The Reynolds stresses are evaluated by employing the SSG Reynolds stress model. For the turbulent heat fluxes $\overline{u_j h}$ the exact transport equation reads:

$$\frac{\partial}{\partial t}\left(\overline{\rho u_i h}\right)+\frac{\partial}{\partial x_j}\left(U_j\overline{\rho u_i h}\right)=\underbrace{-\overline{\rho u_i u_j}\frac{\partial H}{\partial x_j}-\overline{\rho u_j h}\frac{\partial U}{\partial x_j}}_{P_i}\underbrace{-\frac{\partial}{\partial x_j}\overline{\rho u_j u_i h}}_{TD_i}$$
$$\underbrace{-\overline{h\frac{\partial p}{\partial x_i}}}_{TPC_i}+\overline{h\frac{\partial \tau_{ij}}{\partial x_j}}-\overline{u_i\frac{\partial q_j}{\partial x_j}}+\underbrace{\overline{\rho h f_i}}_{\text{external force}} \tag{3}$$

where the production term P_i in eq. (3) can be exactly calculated as a Reynolds Stress model is employed. The turbulent diffusion TD_i contributes to the closure problem and needs therefore additional modeling. TPC_i stands for the correlation between temperature and pressure.

2.1. Turbulent Flux Closure Model

The closure problem for the turbulent flux equation is addressed by applying a gradient diffusion approximation to the turbulent diffusion term TD_i:

$$TD_i=-\frac{\partial}{\partial x_j}\overline{\rho u_i u_j h}=\frac{\partial}{\partial x_j}\left[C_c\frac{k}{\varepsilon}\rho\left(\overline{u_i u_k}\frac{\partial\overline{u_j h}}{\partial x_k}+\overline{u_j u_k}\frac{\partial\overline{u_i h}}{\partial x_k}\right)\right] \tag{4}$$

Neglecting the first term of the right-hand side (r.h.s.) and assuming an isotropic diffusion coefficient, the gradient diffusion term can be further approximated as:

$$TD_i=-\frac{\partial}{\partial x_j}\overline{\rho u_i u_j h}=\frac{\partial}{\partial x_j}\left(\frac{2}{3}C_\Theta\frac{k^2}{\varepsilon}\rho\frac{\partial\overline{u_i h}}{\partial x_j}\right) \tag{5}$$

The TPC_i term can be rewritten as:

$$-\overline{h\frac{\partial p}{\partial x_i}}=\underbrace{-\frac{\partial\overline{hp'}}{\partial x_i}}_{\text{pressure diffusion}}+\underbrace{\overline{p'\frac{\partial h}{\partial x_i}}}_{\text{pressure scrambling}} \tag{6}$$

While the pressure diffusion term can be neglected, the second term can be further split as:

$$\overline{p'\frac{\partial h}{\partial x_i}}=-C_{1\theta}\frac{\varepsilon}{k}\overline{\rho u_i h}-C_{2\theta}\overline{\rho u_j h}\frac{\partial U_i}{\partial x_j} \tag{7}$$

The Boussinesq approximation is further employed, such that fluid properties are considered to be constant and the effect of density differences is taken into account only in the buoyancy term:

$$\overline{\rho h f}_i=-\frac{\rho}{C_p}\beta\overline{h^2}g_i \tag{8}$$

where β is the thermal expansion coefficient. Therefore,

$$\overline{p'\frac{\partial h}{\partial x_i}} = -C_{1\Theta}\frac{\varepsilon}{k}\overline{\rho u_i h} - C_{2\Theta}\overline{\rho u_j h}\frac{\partial U_i}{\partial x_j} + C_{3\Theta}\frac{\rho}{C_p}\beta\overline{h^2}g_i \tag{9}$$

The new resulting unknown quantity is the variance of the enthalpy fluctuation $\overline{h^2}$. The transport equation for this quantity reads:

$$\frac{\partial \overline{h^2}}{\partial t} + \frac{\partial U_j \overline{h^2}}{\partial x_j} = \underbrace{-2\overline{hu_j}\frac{\partial H}{\partial x_j}}_{P_{\Theta\Theta}} - 2\varepsilon_{\Theta\Theta} + \underbrace{\frac{\partial}{\partial x_j}\left(\frac{\nu}{\mathrm{Pr}}\frac{\partial \overline{h^2}}{\partial x_j} - \overline{h^2 u_j}\right)}_{VD_{\Theta\Theta}+TD_{\Theta\Theta}} \tag{10}$$

Where the dissipation $\varepsilon_{\Theta\Theta}$ is expressed by:

$$\varepsilon_{\Theta\Theta} = \frac{\varepsilon}{R}\frac{\overline{h^2}}{2k} \tag{11}$$

R is the ratio between thermal and mechanical turbulent time scale. The viscous term $VD_{\Theta\Theta}$ is instead neglected. The turbulent diffusion term $TD_{\Theta\Theta}$, assuming anisotropy, is expressed as:

$$TD_{\Theta\Theta} = -\frac{\partial}{\partial x_j}\overline{h^2 u_j} = \frac{\partial}{\partial x_j}\left(\frac{2}{3}C_{\Theta\Theta}\frac{k^2}{\varepsilon}\frac{\partial \overline{h^2}}{\partial x_j}\right) \tag{12}$$

Finally, the model transport equation for an incompressible buoyant flow reads:

$$\begin{aligned}\frac{\partial}{\partial t}\left(\overline{\rho u_i h}\right) + \frac{\partial}{\partial x_j}\left(U_j\overline{\rho u_i h}\right) = &-\overline{\rho u_i u_j}\frac{\partial H}{\partial x_j} - \overline{\rho u_j h}\frac{\partial U}{\partial x_j} + \frac{\partial}{\partial x_j}\left(\frac{2}{3}C_\Theta\frac{k^2}{\varepsilon}\rho\frac{\partial \overline{u_i h}}{\partial x_j}\right) - \\ &- C_{1\Theta}\frac{\varepsilon}{k}\overline{\rho u_i h} - C_{2\Theta}\overline{\rho u_j h}\frac{\partial U_i}{\partial x_j} - \left(1 - C_{3\Theta}\right)\frac{\rho}{C_p}\overline{\beta h^2}g_i\end{aligned} \tag{13}$$

$$\frac{\partial \overline{h^2}}{\partial t} + \frac{\partial U_j \overline{h^2}}{\partial x_j} = -2\overline{hu_j}\frac{\partial H}{\partial x_j} - 2\frac{\varepsilon}{R}\frac{\overline{h^2}}{2k} + \frac{\partial}{\partial x_j}\left(\frac{2}{3}C_{\Theta\Theta}\frac{k^2}{\varepsilon}\frac{\partial \overline{h^2}}{\partial x_j}\right) \tag{14}$$

C_c, $C_{1\theta}$, $C_{2\theta}$, C_Θ, $C_{\Theta\Theta}$, are the model constants.

Note that the above model can be applied not only for the energy balance equation and temperature/enthalpy fluctuations, but in general for the transport equation of any passive scalar and corresponding fluctuations. In case that the scalar does not affect the density of the fluid, which is the case in the PSI T-junction experiments used for validation, the buoyancy term in eqs. (9) and (13) is not present.

2.1.1. The epsilon equation

The equation for turbulent heat fluxes is solved together with the SSG model [8] for the Reynolds stresses. Since the turbulent dissipation appears in the equations for the Reynolds stresses, a separate equation for ε is required as well. Employing an isotropic formulation, the

ε-equation reads:

$$\frac{\partial \rho \varepsilon}{\partial t} + \frac{\partial \rho U_j \varepsilon}{\partial x_j} = \frac{\varepsilon}{k}\left(C_{\varepsilon 1} P - C_{\varepsilon 2} \rho \varepsilon\right) + \frac{\partial}{\partial x_j}\left[\left(\mu + \frac{\mu_t}{\sigma_\varepsilon}\right)\frac{\partial \varepsilon}{\partial x_j}\right] \tag{15}$$

In association with the SSG Reynolds stress model, the two coefficients $C_{\varepsilon 1}$ and $C_{\varepsilon 2}$ are assumed to be constant and equal to 1.44 and 1.83 respectively.

3. THE EXPERIMENTAL SET-UP

The test section consists of horizontal T-junction geometry of DN50 Plexiglas pipes [10] (a scheme is reported in Figure 1, left). A series of experiments was carried out [11] by injecting water at different conductivity (tap water and demi-water) in the main and side branches respectively. An assembly of three wire-mesh sensors [12] was mounted at a certain location along the main branch, downstream of the side-branch connection. The sensors record the 2D local instantaneous conductivity of the fluid with a sampling frequency up to 10 KHz and a spatial resolution of 3 mm. The location of the wire-mesh sensors was varied along the main branch. In such a way, high resolved measurements of the mixing scalar and its fluctuations have been recorded at several L/D downstream of the side-branch connection. In addition, velocity measurements were obtained by cross-correlating the scalar fluctuations recorded by the consecutive wire-mesh sensors planes. The obtained time-dependent passive scalar distributions were averaged over a large time interval to provide average profiles with a quite high resolution suitable to the comparison with the CFD calculations. In the experiment used as basis for the present paper, a bulk velocity of 0.5 m/s was employed both for side and main branches. The experimental results were averaged over a period of 10s.

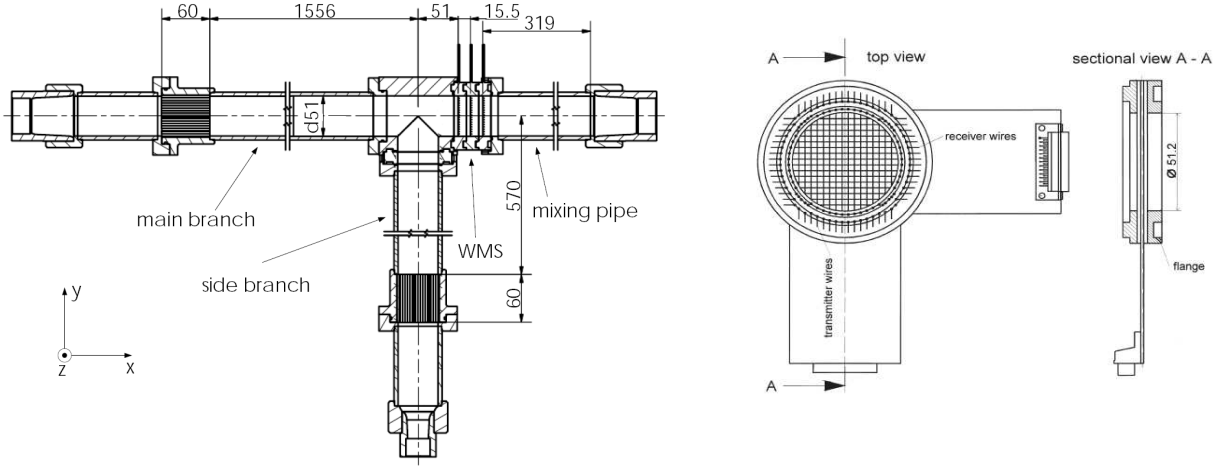

Figure 1 Sketch of the T-junction test section (left) and wire-mesh sensor (right)

4. THE CFD MODEL

For the CFD domain, the side branch and the main branch upstream of the side connection have been modeled by means of 30 cm long pipes. Downstream of the side connection, the pipe extends for additional 60 cm. Turbulent velocity profiles with a cross-section averaged velocity of 0.5 m/s have been imposed at the two branches inlets. At the main branch exit, an outlet boundary condition has been employed.

The domain has been fully meshed with hexahedral elements. Different meshes have been generated to check for mesh convergence. The results reported in the present article have been obtained with a mesh consisting of about 980,000 elements. Details of mesh are shown in Figure 2.

All simulations have been performed by means of ANSYS CFX 11.0. The SSG and the Baseline (BSL) Reynolds Stress models have been adopted, in combination with the turbulent flux transport equation described in the previous chapter. The BSL model [9] is based on the ω-equation, and has therefore the advantage of providing a more accurate near-wall treatment, of importance for wall-bounded flows as the one investigated in the present work.

Since the transport equation for the scalar fluctuations was currently implemented for the energy equation only, slightly different temperatures have been defined at the two T-junctions inlet and the scalar to be compared with the experimental results was defined as:

$$\theta = \frac{T - T_{min}}{T_{max} - T_{min}} = \frac{C - C_{min}}{C_{max} - C_{min}} \tag{16}$$

Here, T are temperatures calculated by ANSYS CFX 11.0 and C concentrations measured by the wire-mesh sensors and obtained by assuming a proportionality of conductivity and salt concentration. As in the experiment there was no density difference between the fluid entering the main and side junction (tap water, desalinated water), respectively, buoyancy effects were not taken into account in the simulations.

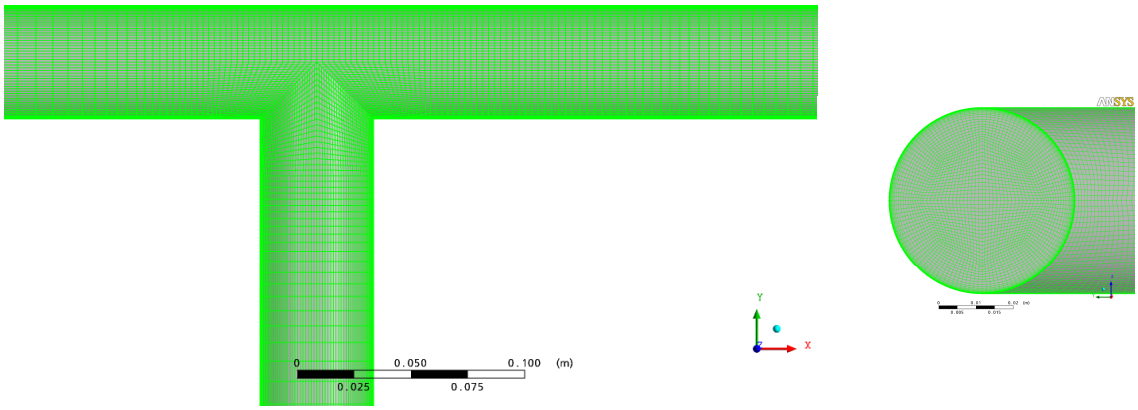

Figure 2 Details of the hexahedral mesh used for the T-junction set-up

5. RESULTS AND DISCUSSION

5.1. The experimental results

Detailed two-dimensional distributions of the time-averaged scalar, scalar fluctuations and axial velocity have been obtained by means of wire-mesh sensors mounted at different locations downstream of the T-junction side connection. A detailed description of the experimental procedure and data evaluation is reported in Ref. [9]. The experimental results of the 2D distributions for scalar, scalar fluctuations and axial velocity, obtained for a bulk velocity of 0.5 m/s in both branches of the T-junction, are shown in Figure 3(a) to Figure 5(a)

respectively. The corresponding profiles along the y-axis (see Figure 2 for the model orientation) are reported in Figure 6.

Focusing on Figure 3(a) and Figure 6 at an L/D = 1, four regions can be identified in the flow after the flow streams from the two sides of the T-junction meet:

a) region where the passive scalar is equal to unity, corresponding to the value of the flow at the inlet of the main T-junction branch;
b) region (around y=0, in Figure 6 for L/D = 1) where the passive scalar is zero, as for the value of the flow at the inlet of the side-connection of the T-junction;
c) mixing region (around $0 < y < 20$ mm);
d) recirculation region ($y < 0$), where entrainment of the main flow into the side flow occurs yielding an increase of the passive scalar above zero.

The scalar fluctuations are the highest in the mixing region. Here the velocity profile is already rather uniform. A strong gradient of the velocity profile is observed in the recirculation region. However, already at an L/D = 1.8 a flat velocity profile for the entire cross-section is obtained, indicating that the extension along the x-axis of the vortexes generated in the recirculation region is relatively short. With increasing L/D, an enhancement of the scalar fluctuations is observed for a larger region of the cross section, corresponding to an extension of the mixing region and therefore to a flattening of the passive scalar profile.

5.2. Performance of Reynolds Stress Model with scalar fluxes fluctuations

A comparison between the SSG and BSL Reynolds Stress Models combined with a transport equation for the scalar fluctuations is presented in Figure 3 to Figure 6. Looking at the 2D velocity distributions (Figure 5), it is clear that both models reproduce the scalar distributions and the RMS profiles in a qualitative way correctly, while over-predicting the axial extension of the recirculation region, where the two vortexes are present, though the BSL model leads to slightly better prediction of the velocity profile.

Both SSG and BSL models exhibit too low diffusion of the passive scalar in the mixing region (see values $0< y < 20$ mm in Figure 6), already at an L/D of 1. In addition, the BSL model significantly over-predicts the entrainment of the passive scalar in the recirculation region ($y < 0$), while the SSG model yields good predictions of θ for $y < 0$. For increasing L/D, though the BSL model leads to an overall better prediction of the passive scalar in comparison to the SSG model, still for both models a scalar value equal to unity is erroneously calculated at y = 25 mm and the qualitative shape of the scalar profile is not correctly captured.

The profile of the scalar fluctuations is well captured by both models for low L/D. However, as the distance from the side connection increases, the extension of the region with high scalar fluctuations is strongly under-predicted by both models.

Quantitative under-prediction of turbulent diffusion is not only found for the transport scalar, but also for the momentum. This is reflected by much higher non-uniformities of the velocity profiles in the calculations. It is clear that this deficiency does not depend on the quality of the scalar fluctuation transport modelling, but it is intrinsic to the Reynolds stress model.

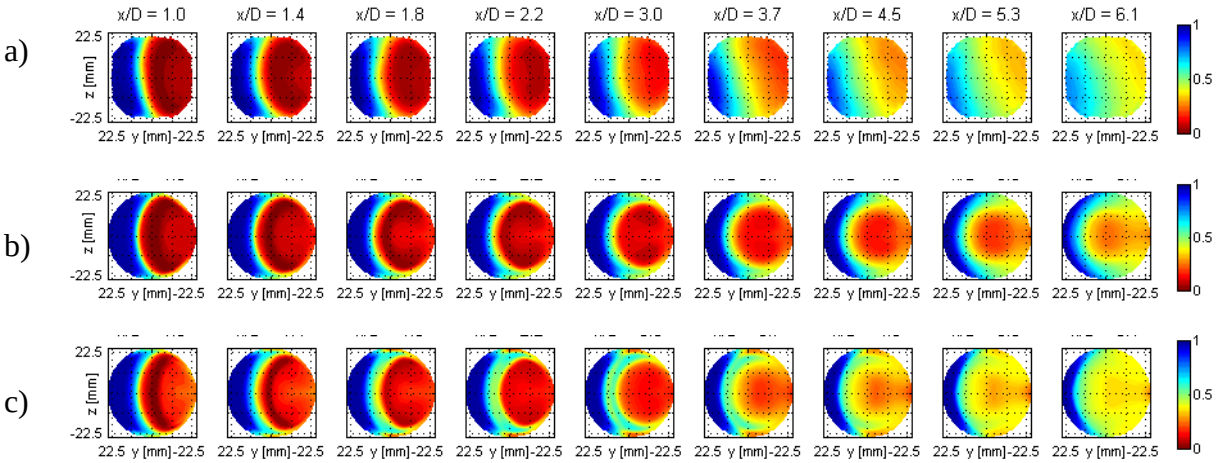

Figure 3 Scalar distributions for different L/D: a) experiments b) SSG model c) BSL model.

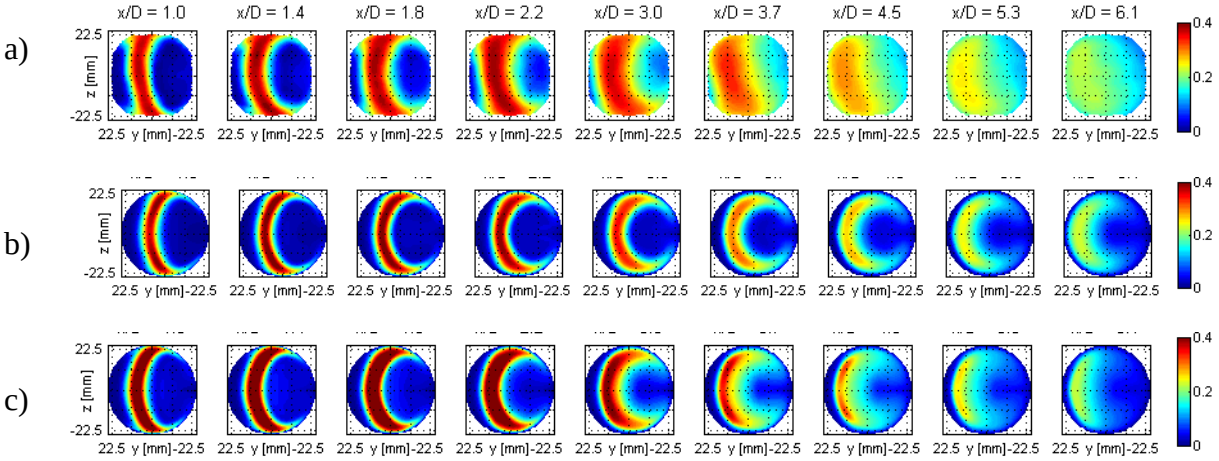

Figure 4 Distributions of scalar fluctuations: a) experiments b) SSG model c) BSL model.

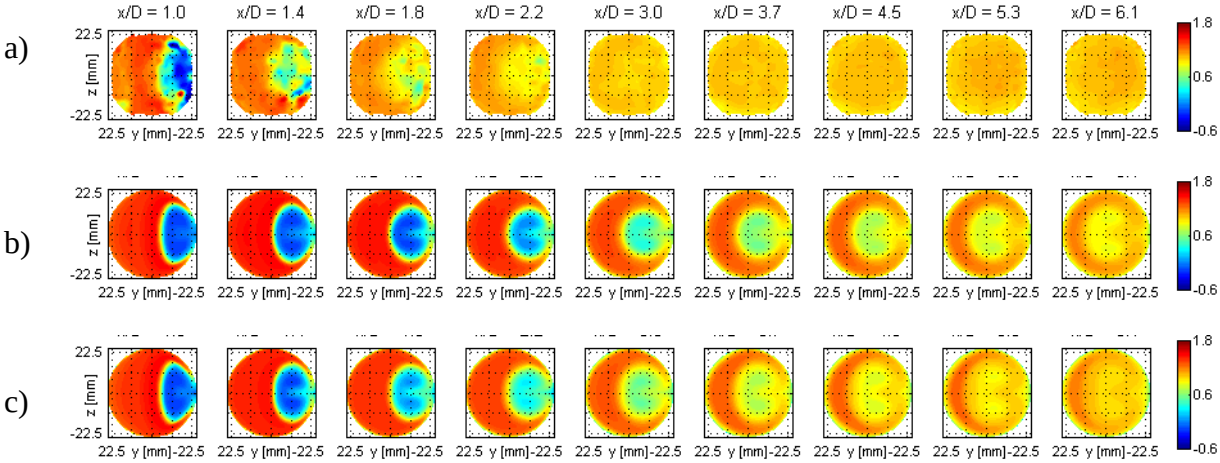

Figure 5 Distributions of axial velocity [m/s]: a) experiments b) SSG model c) BSL model.

5.3. Effect of turbulence dissipation

The calculated scalar profiles obtained at different L/D downstream of the T-junction side-connection indicate an underestimation of the turbulent mixing, regardless of the model employed in the simulation. Previous attempts to improve the predictions of the scalar distribution by means of RANS and URANS simulations have focused on the modification of the turbulent Schmidt number [13, 14], as this has a direct influence on the turbulent diffusion coefficient in the transport equation for the passive scalar. A drastic reduction of the Schmidt number from 0.9 down to 0.1 was necessary in order to enhance the turbulent diffusion such that the experimental results could be better predicted. However, for large L/D the profile of the passive scalar is still not correctly reproduced, even qualitatively [13].

A second very important observation is the lack of turbulent momentum exchange in the calculations. As a matter of fact, the experimental results show that the axial velocity profile reaches a quite uniform distribution much earlier than in the simulations (already at 1.8 L/D from the T-junction side-connection). This means that the underestimation of the turbulent mixing is due to a too low turbulent kinetic energy, which causes both transport scalar diffusion and momentum exchange to be under-predicted. A manipulation by decreasing the Schmidt number can only affect the scalar mixing without improving the decay of the non-uniformity of the velocity profiles due to turbulent momentum exchange. The often applied Schmidt number fitting is therefore a curing of symptoms rather that an elimination of the real causes of the model deficiencies.

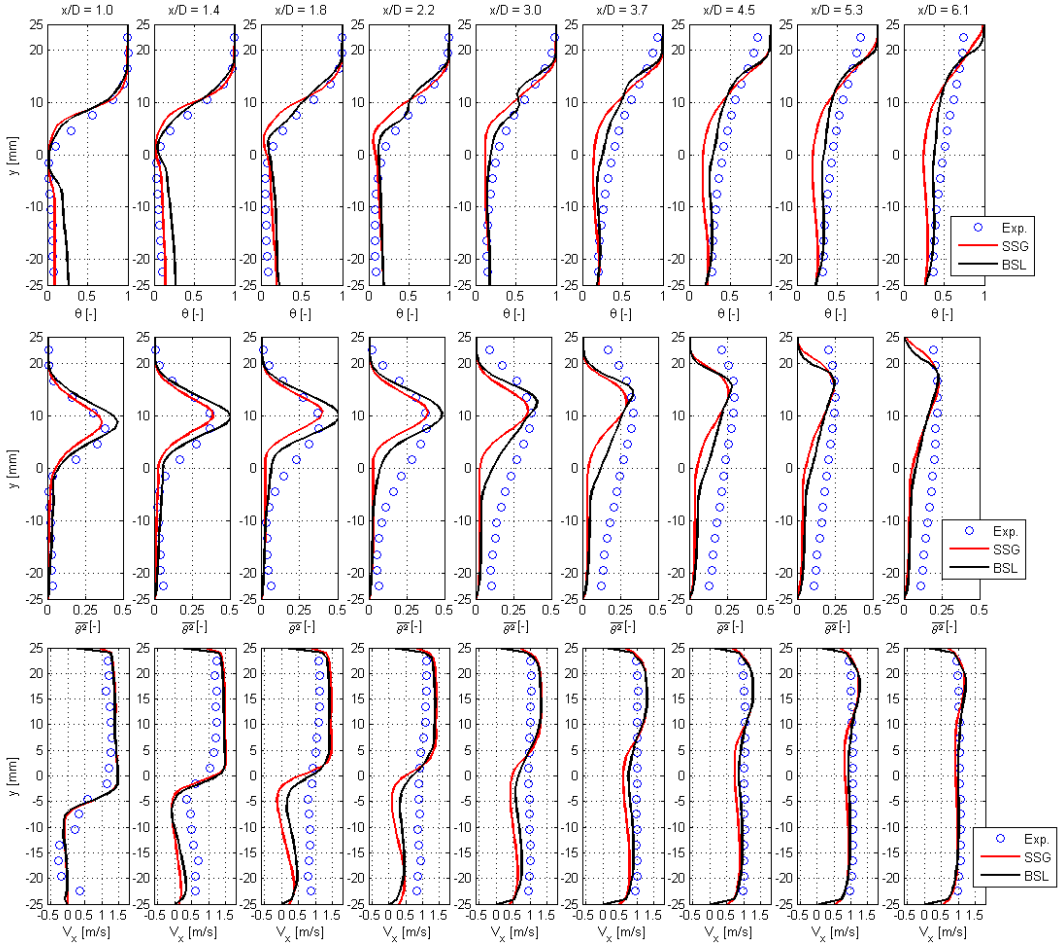

Figure 6 Profiles of scalar, scalar fluctuations and axial velocity at different L/D.

In Ref. [5] Prasser and co-workers propose an increase of C_μ in the k-ε model in order to enhance both turbulent mixing and turbulent momentum exchange by fitting only one parameter. They clearly indicate that this cannot be envisaged as the final approach to solve the problem, because the lack in turbulent kinetic energy can have a more fundamental origin in a number of other model constants, which requires more detailed investigations. In a Reynolds stress model, such model coefficient like C_μ does not exist, since the components of the turbulent stress tensor are exact balance quantities.

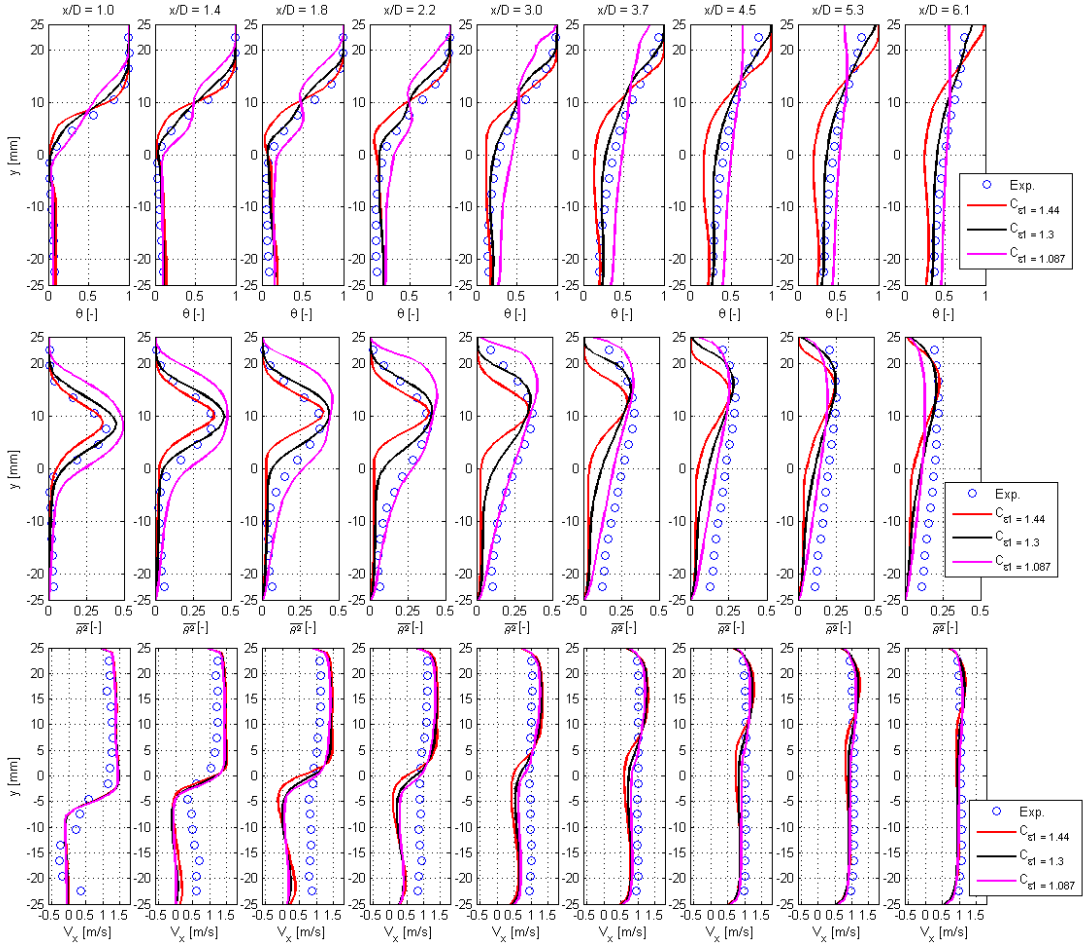

Figure 7 Profiles of scalar, scalar fluctuations and axial velocity for different values of $C_{\varepsilon 1}$.

Here, one way to increase the momentum exchange consists in decreasing the turbulent dissipation. A sensitivity study has been performed by varying the coefficient $C_{\varepsilon 1}$, which multiplies the production term in the equation for the turbulent dissipation. The default value of 1.44 has been decreased down to 1.3 and 1.087 respectively. The results are presented in Figure 8 to Figure 10. A clear improvement in the prediction of the scalar profile for all values of L/D is already obtained when a value $C_{\varepsilon 1} = 1.33$ is employed, corresponding to a decrease of $C_{\varepsilon 1}$ of 7.6%. Improvements for the scalar fluctuations are obtained as well, though for large L/D an underestimation can be observed in comparison to the experimental values.

Decreasing further the $C_{\varepsilon 1}$ coefficient leads to a too strong diffusion of the passive scalar, without any additional improvements in the velocity profile or in the profile of the scalar fluctuations.

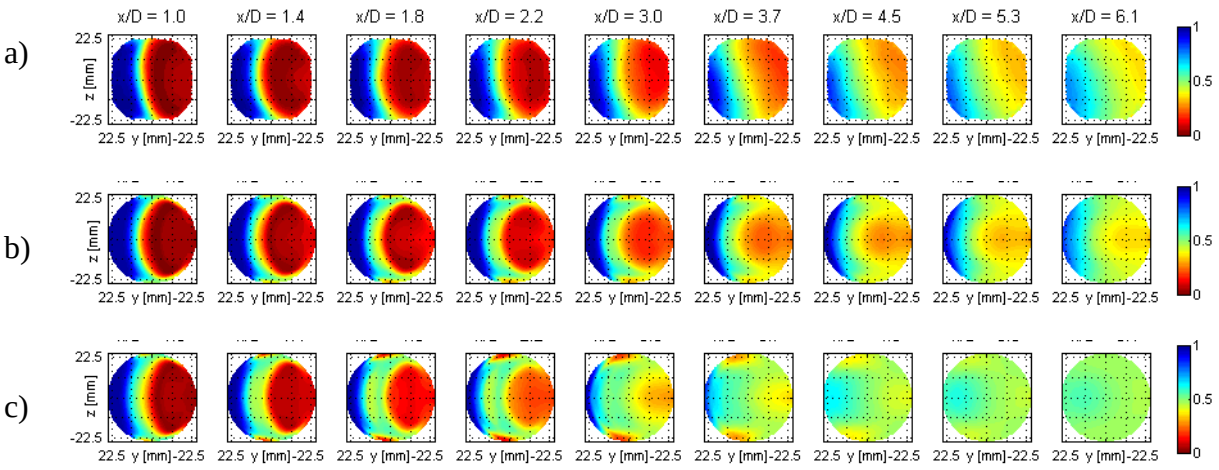

Figure 8 Scalar distributions: a) Experiment; b) $C_{\varepsilon 1}$= 1.3; c) $C_{\varepsilon 1}$= 1.087.

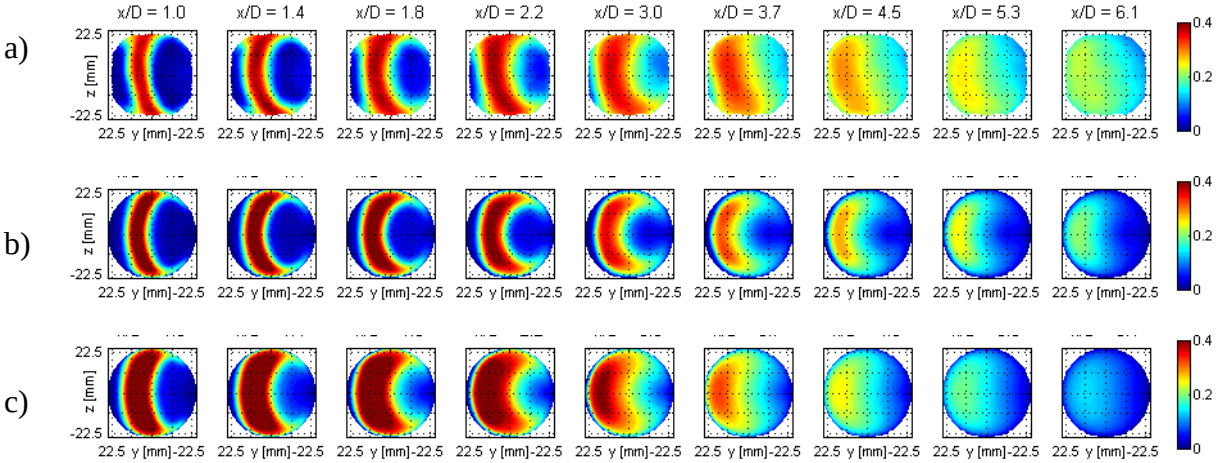

Figure 9 Distributions of scalar fluctuations: a) Experiment; b) $C_{\varepsilon 1}$= 1.3; c) $C_{\varepsilon 1}$= 1.087.

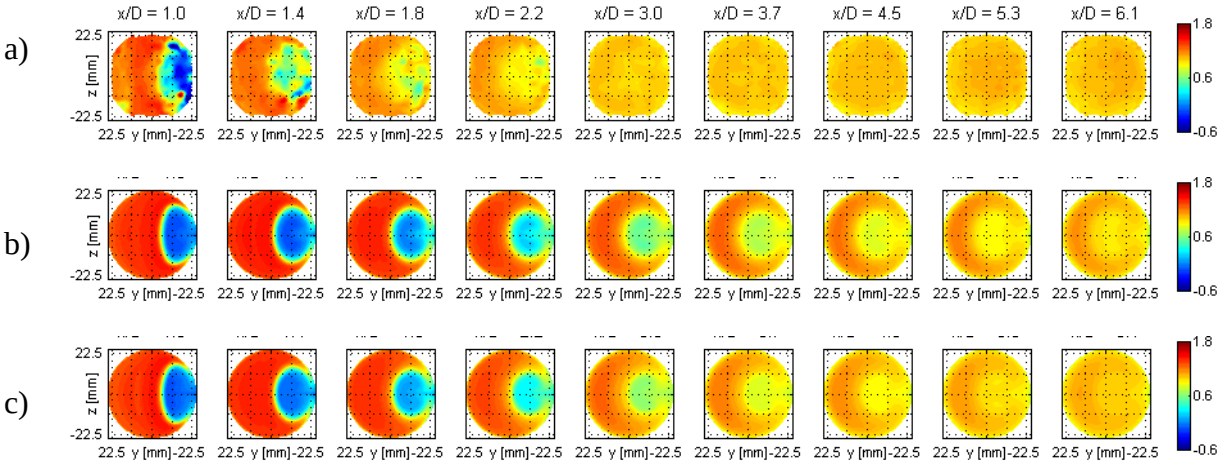

Figure 10 Axial velocity distributions [m/s]: a) Experiment; b) $C_{\varepsilon 1}$= 1.3; c) $C_{\varepsilon 1}$= 1.087.

It has to be made sure that manipulations of the model coefficients do not affect the quality of the turbulence model in the boundary layer too much. As an integral quantity resulting from wall shear stresses, the pressure drop along the main flow path in the T-junction was analysed. It was checked to which extend the manipulation of $C_{\varepsilon 1}$ had caused a change of the pressure drop.

In Figure 11 (left) the pressure distribution along the T-junction main axis is reported for the simulations obtained with the SSG model by varying the $C_{\varepsilon 1}$ coefficient. As expected, the strongest influence is obtained for the region soon after the connection of the T-junction with the side connection (x=0). This is the region where the vortex develops forming a recirculation region. For the pipe section before the side connection, the pressure profile corresponds to a developed turbulent flow with bulk velocity of 0.5 m/s. By analyzing the pressure drops in this region (Figure 11, right) it is possible to observe that the change in the $C_{\varepsilon 1}$ coefficient from 1.44 to 1.3 yields a decrease of the pressure drop of less than 2%. It can be therefore concluded that such a decrease of the turbulent dissipation does not affect significantly the behaviour of the flow in the boundary layer.

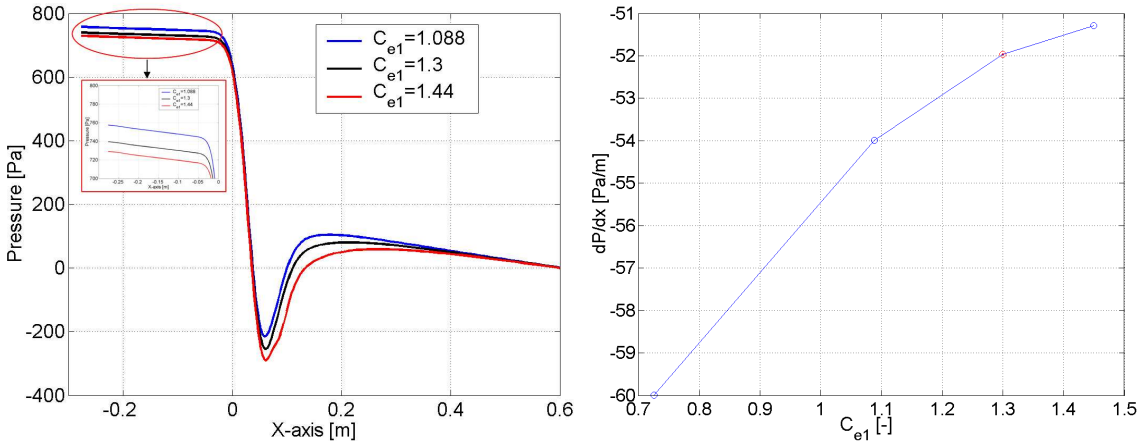

Figure 11 Pressure distribution (left) and pressure gradient as function of $C_{\varepsilon 1}$ (right).

6. CONCLUSIONS

Reynolds stress turbulent models combined with scalar fluctuation transport equations offer the opportunity to quantify temperature fluctuations by efficient steady-state RANS simulations. This is of great advantage in comparison to LES simulations or unsteady RANS, especially in view of applications to the assessment of thermal fatigue of large components, which are typical in nuclear power plants. The results presented in this paper are rather promising. However, for successful predictions of the temperature fluctuations, improvements of the equation for the dissipation rate currently employed in commercial CFD codes are clearly needed. As a matter of fact, it has been shown that an improvement in the estimation of the Reynolds stresses yields a considerable gain in the estimation of the scalar (temperature) fluctuations. In the past, it has already been recognized that a formulation of the dissipation transport equation with constant coefficients is too simple and yields unsatisfactory results in complex flows [15]. Therefore, the next step will be to combine the fluctuations scalar transport equation with a more suitable equation for the turbulence dissipation.

A further challenge is the development of methods to assess the frequency characteristic of the temperature fluctuations, by adopting information on the turbulence scale taken from the relation between turbulent kinetic energy and turbulent dissipation. Such information is necessary to assess the relevance of fluctuations to fatigue, since only low-frequency fluctuations in the fluid can induce large temperature changes in the walls. Another open issue is the coupling to a heat conduction model for the wall.

REFERENCES

1. L.-W. Hu and M.S. Kazimi, "LES benchmark study of high cycle temperature fluctuations caused by thermal striping in a mixing tee", *Int. J. Heat and Fluid Flow*, **27**, pp. 54 – 64 (2006).
2. S.K. Kang, K. Takeyama, Y.A. Hassan, "CFD Analysis of Thermal Mixing in T-junction with Elbow Upstream", *Transaction of American Nucl. Society*, **97**(1), pp. 420 – 421 (2007).
3. P. Coste, P. Quemere, P. Roubin, P. Emonot, M. Takanaka, H. Kamide, "Large Eddy Simulation of highly Fluctuational Temperature and Velocity Fields Observed in a Mixing-tee experiment", *Nucl. Technology* , **164**, pp. 76 – 88 (2008).
4. J. Simoneau, J. Champigny, O. Gelineau, "Applications of large eddy simulations in nuclear field", *Nucl. Eng. Des.*, in press, http://dx.doi.org/10.1016/j.nucengdes.2008.08.018 (2008).
5. H.-M. Prasser, A. Manera, B. Niceno, M. Simiano, B. Smith, C. Walker, R. Zboray, "Fluid mixing at a T-junction", *Proc. of Experiments and CFD Codes Application to Nuclear Reactor Safety (XCFD4NRS)*, OECD/NEA and IAEA Workshop, Grenoble, France, Sept. 10-12 (2008).
6. J. I. Lee, L Hu, P. Saha, M.S. Kazimi, "Numerical Analysis of Thermal Striping induced high cycle thermal fatigue in a mixing tee", *Nucl. Eng. Des.*, **239**(5), pp. 833 – 839 (2009).
7. R. Lechner, F. Menter, "Transport Equation for Turbulent Heat Fluxes including Buoyancy Effect", Presentation ETH Zurich, 25 February (2008).
8. C.G. Speziale, S. Sarkar, T.B. and Gatski, "Modelling the pressure-strain correlation of turbulence: an invariant dynamical systems approach", *J. Fluid Mechanics*, **277**, pp. 245-272 (1991).
9. ANSYS CFX-11, Solver Theory Guide, ANSYS Inc. (2006).
10. R. Zboray, A. Manera, B. Niceno, H.-M- Prasser, "Investigations on Mixing Phenomena in Single-Phase Flows in a T-Junction Geometry", *Proc. of NURETH-12*, Pittsburgh, Pennsylvania, U.S.A. September 30-October 4, paper 71 (2007).
11. C. Walker, M. Simiano, R. Zboray, H.-M Prasser, "Investigations on mixing phenomena in single-phase flow in a T-junction geometry", *Nucl. Eng. Des.*, **239**(1), pp. 116-126 (2008).
12. H.-M Prasser, A. Bottger, J. Zschau, "A new electrode-mesh tomograph for gas-liquid flow", *Flow Meas. and Instr.*, **9**, pp.111-119 (1998).
13. C. Walker, A. Manera, B. Niceno, M. Simiano, H.-M Prasser, "Steady-state RANS-Simulations of the Mixing in a T-junction",Submitted to *Nucl. Eng. Des.*, (2008).
14. Th. Frank, M. Adlakha, C. Lifante, H.-M Prasser, F. Menter, "Simulations of Turbulent and Thermal Mixing in T-junctions using URANS and Scale-Resolving Turbulence Models in ANSYS CFX", *Proc. of Experiments and CFD Codes Application to Nuclear Reactor Safety (XCFD4NRS)*, OECD/NEA and IAEA Workshop, Grenoble, France, Sept. 10-12 (2008).
15. B. Launder, N. Sandham, "Closure strategies for turbulent and transitional flows", *Cambridge University Press*, (2002).